New correlations for focusing effect evaluation of the light metal layer in the lower head of a nuclear reactor in case of severe accident

F. Rein, Florian Fichot, Laure Carénini, Michael Le Bars, B. Favier

New correlations for focusing effect evaluation of the light metal layer in the lower head of a nuclear reactor in case of severe accident

Rein F, Fichot F, Carénini L
Institut de Radioprotection et de Sûreté Nucléaire (IRSN)
BP3 – 13115 St Paul lez Durance - FRANCE
florian.rein@irsn.fr, florian.fichot@irsn.fr, laure.carenini@irsn.fr

Le Bars M, Favier B
Aix Marseille Univ, CNRS, Centrale Marseille, IRPHE, Marseille, 13013, FRANCE
michael.le-bars@cnrs.fr, benjamin.favier@cnrs.fr

ABSTRACT

In case of a severe accident (SA) in a nuclear reactor, the core heats up and materials melt and relocate to the lower head of the vessel. In such configuration, stratification occurs between the oxide and metal phases present in the melt. When the metal phase is lighter than the oxide phase, the maximum heat flux applied to the vessel wall is concentrated at the location of this top metal layer, creating the so-called "focusing effect". The modelling of the focusing effect is essential for SA codes to properly evaluate the vessel failure time or to demonstrate the vessel integrity, when In Vessel Retention (IVR) strategy is implemented. However, existing correlations used in SA codes for focusing effect modelling have some limitations: if the thickness of the metal layer becomes very small, they predict an extremely high heat flux. Moreover, they were validated with tests using water, whereas the Prandtl number was found to play a significant role in this heat transfer.
In this paper, the focusing effect is studied based on 3D Direct Numerical Simulations (DNS) of a cylindrical metal layer, covering all possible metal layer characteristics in terms of geometry and boundary conditions, especially for its top surface where the intensity of radiative heat transfer may vary. The analysis of the fluid behavior and the quantitative results obtained allow to derive new correlations and a new model based on the radial profile of the mean temperature of the system and on the radial profile at the top surface. Results at reactor scale confirm the overestimation of existing 0D model used in SA codes for a thin metal layer and highlight the relevance of the proposed model for focusing effect evaluation during transient situations.

KEYWORDS
Focusing effect, DNS, heat transfer correlation, SA codes

1. INTRODUCTION

In a light water nuclear reactor, if it is not possible to cool down the fuel in the core of the vessel, a Severe Accident (SA) will happen, characterized by the melting of fuel rods and of the surrounding structures. The melt formed, called corium, will relocate to the lower plenum of the vessel. It is mainly composed of Uranium dioxide, partially oxidized zirconium and steel. The study of the corresponding quaternary system U-O-Zr-Fe, associated with the results of the OECD MASCA 1 and 2 programs [1], reveals that a gap of miscibility exists between the oxide and metal phases. Due to the melt stratification in the lower plenum, heat flux profile applied to the vessel wall will be impacted. In the most generic case when the metal phase is lighter than the oxide, it will lay on top of the oxide pool and concentrate, along its external surface, the

heat coming from the oxide pool where the residual power is generated. This phenomenon is known as "focusing effect" and may lead to the most critical configurations when studying the vessel integrity. As a consequence, it is of tremendous importance for SA codes to accurately estimate the heat transfer in the top metal layer. Up to now, correlations used in SA codes for focusing effect modelling come from the work performed in the scope of the demonstration of the applicability of In Vessel Retention (IVR), by external cooling, as a severe accident management strategy [2]. However, this approach has shown some limitations, which are discussed in the first part of this paper. Then, results of 3-Dimensional (3D) Direct Numerical Simulations (DNS) of the top metal layer of a stratified corium pool are used with the following objectives: (i) understand the behavior of the fluid and of the heat transfer for the different layer characteristics which can be reached in the reactor case, (ii) derive scaling laws and finally (iii) build up a model usable in integral SA codes. In the last part, the results obtained with the new correlations and approach are presented and discussed, especially regarding former modelling.

2. CHALLENGES ASSOCIATED WITH FOCUSING EFFECT MODELLING: CURRENT STATUS IN SEVERE ACCIDENT CODES AND LIMITATIONS

The situation of interest for the focusing effect is a cylindrical liquid layer of thickness H and radius R, uniformly heated from below due to the heat flux from the oxide pool $\hat{\phi}$ and cooled along the lateral side, where the melting of the vessel wall imposes at maximum the liquidus temperature of steel $\hat{T}_0$. In addition, the top boundary condition corresponds to a radiative heat transfer $\hat{\phi}_{up}$ which depends on the geometry and temperature of the surrounding structures (cf. Figure 1). It is worth noting that, since in most of the reactor designs with IVR strategy, the corium pool is expected to reach the cylindrical part of the vessel, configuration with non-vertical vessel wall was not studied yet and is out of the scope of this paper.

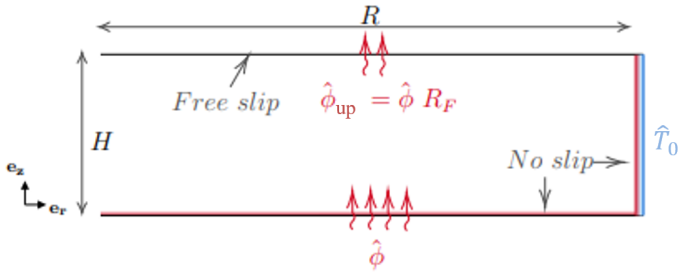

Figure 1. Sketch of the metal layer in a vertical plane through the cylinder.

In the first studies developed by Theofanous for the IVR strategy [2], the focusing effect was studied considering two distinct components for the heat transfer in the layer based on classical natural convection correlations:

- Globe and Dropkin correlation [3] for vertical heat transfer, referring to the study of heat transfer between two horizontal plates, the lower one being heated.
- Churchill and Chu correlation [4] for horizontal heat transfer, referring to the study of heat transfer through a vertical wall cooled by an ambient fluid.

The assumption of a well-mixed fluid in the bulk was made, as well as of symmetry for the vertical heat transfer: the vertical temperature difference between the bottom and the bulk temperatures is assumed equal to the vertical temperature difference between the bulk and the top temperatures. Applicability of those assumptions and the validity of this modelling for conservative focusing effect evaluation were confirmed with the results of the MELAD experiments [5], whose characteristics are presented in Table I.

The extension of the validity of this approach was then studied thanks to the tests performed in the BALI-metal facility [6]. The main idea was to study heat transfer for higher aspect ratios (Γ=R/H) from 5 to 40.

Indeed, initially the study was performed for a "bounding" case supposed to be the one reached at steady state once all materials have been melted and leading to the maximum residual power in the molten pool. In such cases, the amount of molten steel incorporated in the metal phase would be large enough to avoid a shallow layer configuration. However, considering transient effects in corium stratification process has shown that the maximum heat flux at the outer surface of the vessel wall may be reached before reaching the steady state [7]. It emphasizes the necessity to deal with any possible metal layer height in SA codes, especially for the cases where stratification inversion occurs. In addition, in the BALI-metal test, for the top boundary condition, conduction through an epoxy plate and then heat exchanger at imposed temperature was used in order to be more representative of the reactor case with the top radiative heat transfer condition compared to the imposed temperature used in MELAD experiment. The results of BALI-metal tests show that, for shallow layer thickness (aspect ratio above 10), the 0D model developed initially is conservative and overestimates the focusing effect.
More recently, HELM [8] and HELM-LR [9] experiments were performed in a cylindrical test section with the objective of extending the initial approach developed by Theofanous [2] respectively to lower and higher aspect ratios as synthetized in Table I.

Table I. Synthesis of experiments performed for the focusing effect

Name	Geometry	Fluid	Top boundary condition	Aspect ratio $\Gamma=R/H$	R (m)	H (m)
MELAD	Rectangular	Water	Imposed temperature	5	0.5	0.1
BALI-metal			Conduction through epoxy plate	5-40	2	0.05-0.4
HELM	Cylindrical		Imposed temperature	1.25-2.5	0.5	0.2-0.4
HELM-LR				3.125-12.5		0.04-0.16
Reactor case		Metal	Radiative heat transfer	1-∞	2	0-2

Looking at the comparison between available tests and the reactor case (cf. Table I), it appears that the main discrepancy between experiments and reactor case lies in the choice of the simulant. To overcome this difficulty, numerical simulations with Computational Fluid Dynamics (CFD) codes of the metal layer were performed within the European IVMR project [10]. They concluded on a significant effect of the fluid properties (water versus steel) on the global phenomenology, particularly the Prandtl number: the lateral heat flux and concentration factor, being up to 50% higher with steel for similar boundary conditions. The temperature field appeared to be much more controlled by diffusive effects, which is easily understandable considering that the Prandtl of metal is significantly lower than the Prandtl of water (0.1 versus 5). The validity of results obtained with water as a simulant material for the metallic layer is thus questionable as well as the model derived so far for SA integral codes.
In [10] new correlations based on CFD calculations results were also proposed. However, they reveal a difficulty with the consideration of the top boundary radiative transfer. Indeed, this condition plays a major role on the heat transfer in the metal layer and was introduced in the correlation by means of a homogeneous surface temperature. However, a radial variation of the surface temperature in the metal layer can be expected due to the combination of the side cooling and of the bottom heating. Consequently, it appears necessary to well estimate this top boundary condition and the associated radiative heat flux $\hat{\phi}_{up}$. The difficulty of this problem is that $\hat{\phi}_{up}$ depends on the surface temperature, which depends on the heat transfer in the metal, which depends on $\hat{\phi}_{up}$. Therefore, the solution is implicit. To try to simplify this problem, the proposed approach in this paper is to prescribe the top heat flux and to examine the temperature profiles to

understand the fluid behavior and associated heat transfer and correlate them with the driving parameters of the flow. This approach was also followed in [11] but turbulence parameters used in the performed CFD simulations lead to significant uncertainties.

3. 3-DIMENSIONAL MODELLING OF THE METAL LAYER WITH DIRECT NUMERICAL SIMULATIONS

3.1. Problem Definition

A parameter R_f is introduced as the fraction of total power lost at the top boundary, representing the integral of the radiative power over the top surface of the layer. It will allow describing all the different metal layer configurations which may be encountered in the reactor case as discussed in the previous paragraph. The fluid is considered incompressible and the Oberbeck-Boussinesq approximation is made.
The dimensionless conservation equations of the momentum (1), mass (2) and energy written as a function of temperature (3), are therefore:

$$\frac{1}{Pr}(\partial_t \boldsymbol{V} + (\boldsymbol{V}.\nabla)\boldsymbol{V}) = -\nabla P + Ra_\phi T \boldsymbol{e_z} + \nabla^2 \boldsymbol{V} \quad (1)$$

$$\nabla.\boldsymbol{V} = 0 \quad (2)$$

$$\partial_t T + (\boldsymbol{V}.\nabla)T = \nabla^2 T \quad (3)$$

assuming the following scaling based on a diffusive time, for non-dimensional variables:

$$r = \frac{\hat{r}}{H}, \quad z = \frac{\hat{z}}{H}, \quad t = \frac{\kappa}{H^2}\hat{t}, \quad \boldsymbol{V} = \frac{H}{\kappa}\hat{\boldsymbol{V}}, \quad P = \frac{H^2}{\rho\nu\kappa}\hat{P}, \quad T = \frac{k}{\hat{\phi}H}\left(\hat{T} - \hat{T}_0\right) \quad (4)$$

Here and for the rest of this paper, $\hat{}$ represents a dimensional variable and ρ, ν, κ, β, k, $\hat{P}$ and $\hat{T}$ represent the density, kinematic viscosity, thermal diffusivity, thermal expansion coefficient, thermal conductivity, pressure and temperature of the fluid respectively. $\boldsymbol{e_z}$ is the unit vector in vertical direction. The radial ($\hat{r}$), azimuthal ($\hat{\varphi}$) and vertical ($\hat{z}$) components of the velocity $\hat{\boldsymbol{V}}$ are denoted by $\hat{u}$, $\hat{v}$ and $\hat{w}$ respectively. On the bottom and the side no slip conditions are considered, while a free slip condition is applied on the top surface. Indeed, an oxide crust is expected to be formed at the bottom of the metal layer but not at its top surface.

$$\forall r, \quad z = 0, \quad u = v = w = 0 \text{ and } \partial_z T = -1 \quad (5)$$

$$\forall r, \quad z = 1, \quad \partial_z u = \partial_z v = w = 0 \text{ and } \partial_z T = -R_f \quad (6)$$

$$\forall z, \quad r = \Gamma, \quad u = v = w = 0 \text{ and } T = 0 \quad (7)$$

To describe the problem, 4 non-dimensional input parameters are required. The aspect ratio Γ, the flux ratio R_f, the Rayleigh number Ra_ϕ which is based on the heat flux imposed at the bottom, and the Prandtl number Pr fixed to 0.1 throughout the paper and corresponding to the prototypical liquid metal.

$$\Gamma = \frac{R}{H}, \quad R_f = \frac{\hat{\phi}_{up}}{\hat{\phi}}, \quad Ra_\phi = \frac{\beta g \hat{\phi} H^4}{k\nu\kappa}, \quad Pr = \frac{\nu}{\kappa} = 0.1 \quad (8)$$

The computational solution of the governing equations (1)-(3) and boundary conditions (5)-(7) is performed using Nek5000 [12].
For discretization, the cylindrical geometry is divided up to 36608 hexahedral elements, refined near boundaries to accurately capture viscous and thermal boundary layers. Within each element, velocity is

discretized using Lagrange polynomial interpolants based on tensor-product arrays of Gauss–Lobatto–Legendre quadrature points. The polynomial order N varies between 6 and 10 across elements in this study. Nonlinear products are computed employing the 3/2 rule for dealiasing, where an extended dealiased polynomial order of 3N/2 is utilized. Time stepping employs a third-order approach using a mixed explicit-implicit backward difference scheme.

3.2. Results of Numerical Simulations

Up to 70 numerical simulations were performed in order to cover the different values of the parameters R_f in [0-0.9], Ra_ϕ in [10^2-10^9] and Γ in [4-16]. A total CPU time of more than 4 million hours was necessary for these simulations. For high Rayleigh number $Ra_\phi = 10^9$ and high aspect ratio ($Ra_\phi \geq 10^8$ and $\Gamma \geq 8$) a 10% filter is applied on the 2 last modes [12]. Simulations for these particular cases correspond to Large Eddy Simulation (LES) and not DNS but it should be noticed that, in the system studied, the Prandtl number is low, meaning that the filter does not impact the thermal aspect but only the viscous dissipation at small scale. The study of higher Rayleigh number corresponding to thicker metal layer (around 10^{12} for metal layer of about 60cm) as well as larger aspect ratio (40 for metal layer of 5cm) is not possible with this DNS approach (excessive computation time) and thus extrapolations will have to be made to cover all the configurations which have to be evaluated in reactor case. To justify the validity of such approach, in combination with this numerical work, an experimental device named FOCUS was set up with a simulant gas having representative Prandtl number and tests are carried out with this objective of confirming the extrapolation of this modelling at Rayleigh number reaching about two orders of magnitude above the maximum value reached in DNS (up to $Ra_\phi = 10^{10}$).

Firstly, the case with low top heat transfer is studied, imposing R_f=0.1 in order to understand the heat transfer with the cooled side wall. This case is expected to be reached in the reactor case as soon as the metal layer temperature is close to the one of the surrounding structures. An example of temperature field and velocity streamlines is presented in Figure 2 (left). A radial temperature gradient is visible between the center and the cooled lateral side. The fluid circulates from the bottom to the top in the center and then horizontally, at the top, from the center to the side wall and, at the bottom, from the side wall to the center. A 3D instability is observed of figure 2, breaking the azimuthal symmetry and forming large-scale patterns in both the temperature field and the streamlines. In the following, all numerical results were obtained after reaching a statistically stationary steady state and subsequently averaging over time. Further information regarding the numerical methodologies and convergence criteria can be found in [13].

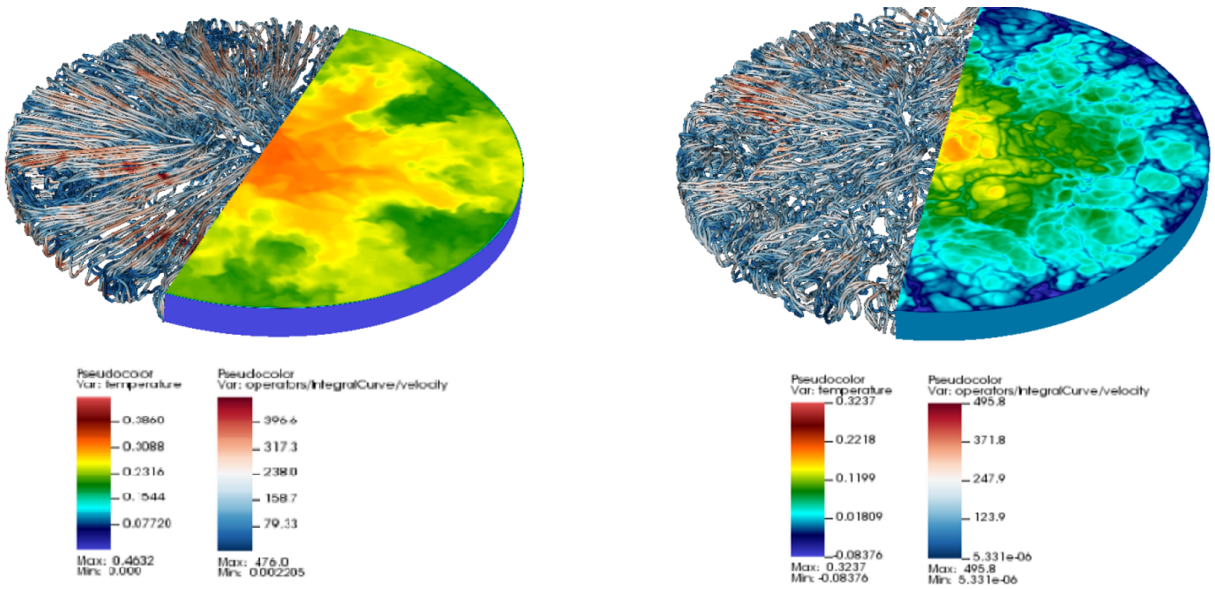

Figure 2. Snapshot of the 3D view showing the top surface temperature field on the right half cylinder and the velocity streamlines on the other half, for $\Gamma = 8$, $Ra_\phi = 10^7$ and $R_f = 0.1$ (left), $R_f = 0.9$ (right).

The analysis of the radial temperature profile (averaged in z and φ and noted with an overbar) exhibits two zones as illustrated in the top of Figure 3: A zone close to the lateral cooled wall where the average temperature is uniform (except in the boundary layer of course) and a zone in the center where the temperature increases linearly towards the center. The analysis of the velocity field for the case $R_f = 0.1$ (cf. Figure 4 a)) confirms the presence of these two zones at the same time as the global circulation of the fluid in all the cylinder already identified in Figure 2. The external zone appears to be directly associated to the presence of the cold tongue formed at the cooled wall and already identified in previous experimental and numerical works [6], [10]. Increasing the Rayleigh number increases the extension of this zone where the temperature is uniform near the cooled wall. This can be interpreted considering the balance between the horizontal motion governed by inertia generated by the downwards fluid coming from the cold wall and the fluid friction with the bottom. In Figure 3, it is also shown that the separation between the two zones can be well determined based on the identification of the location where the sign of the radial pressure gradient changes.

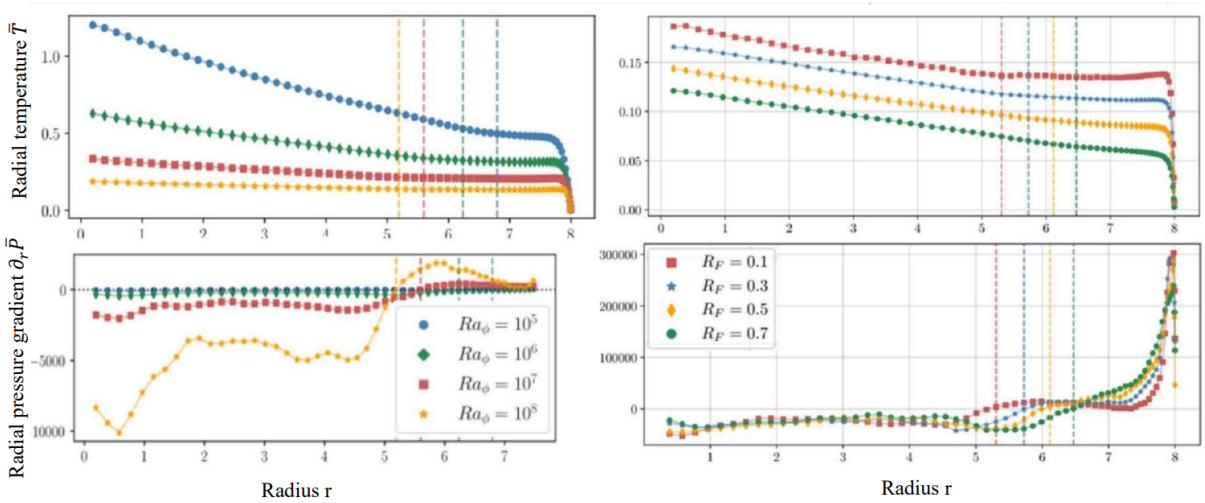

Figure 3. Radial temperature profile (top) and radial pressure gradient (bottom) depending on the Rayleigh number for (Γ=8, R_f = 0.1) (left) and on the heat flux ratio for (Γ=8, $Ra_\phi = 10^8$) (right). Identification of the delimitation between the zone affected by the cooled wall and the rest of the fluid.

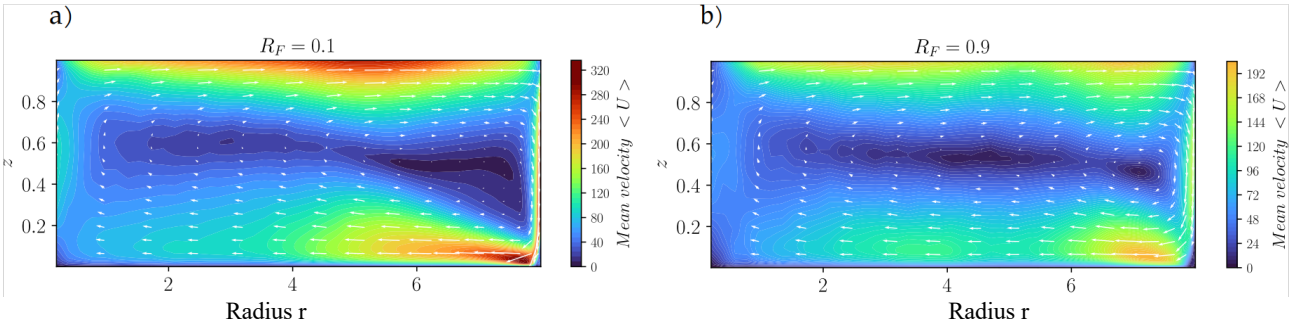

Figure 4. Axial cut of the velocity field for Γ = 8, $Ra_\phi = 10^7$ and a) R_f = 0.1, b) R_f = 0.9.

The impact of an increase of the top heat flux (R_f parameter) on the radial temperature profile is further illustrated in Figure 5. It is shown that for the extreme case when R_f=0.9, the zone with uniform temperature near the lateral cooled wall is significantly reduced and the temperature decreases radially at a constant rate in the other zone. One important point to notice is that the top temperature is lower than the average one in this case: therefore, it is not stable, and the circulation is disturbed by instabilities as shown in Figure 2 (right). The heat transfer to the top surface is driven by the vertical temperature gradient in the layer, as in Rayleigh-Bénard convection. However, even in this extreme configuration where only 10% of the power is transferred through the lateral cooled wall, the global circulation of the fluid along the cylinder boundaries is still present as illustrated in Figure 4b) despite turbulent fluctuations now reaching a comparable magnitude to this mean flow (not shown).

For the intermediate case R_f=0.5, the two previously identified zones can also be distinguished but the "plateau zone" is smaller compared to the case with R_f=0.1: the extent of this region is directly associated to the intensity of the lateral heat flux, which agrees with the proposed interpretation given previously for the effect of the Rayleigh number. Further results and more detailed analysis and interpretation of these simulations are available in [13].

3.3. Correlations derived for the radial profile of the temperature

Considering the analysis of the two zones identified in the radial temperature profile and on its simple shape, it is proposed to derive scaling laws from available numerical results in order to evaluate this radial temperature profile in the layer depending on the characteristics of the flow Ra_ϕ, R_f, Γ. As illustrated in Figure 6, the temperature profile can be described by the following 3 parameters: the temperature in the plateau zone near the cooled wall T_p; the slope of the temperature profile in the linear region ($-s_p$); and the length of the decreasing temperature zone r_p.

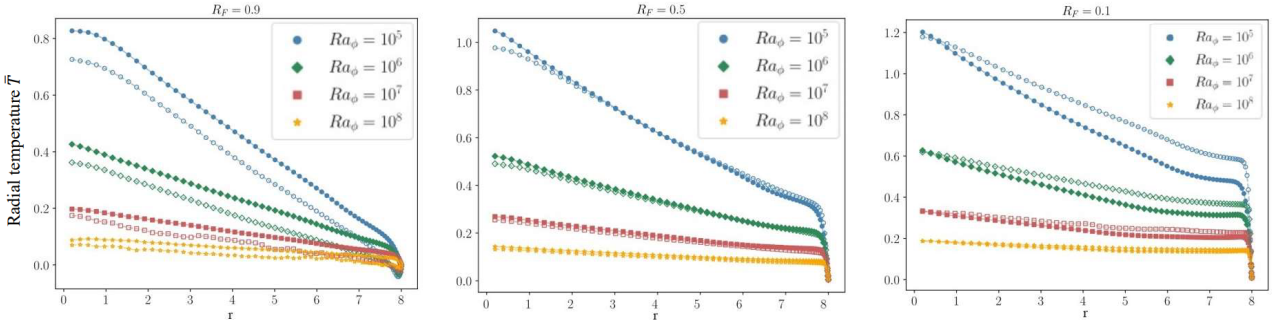

Figure 5. Radial temperature profile depending on Ra_ϕ and for three different heat flux ratios (R_f=0.9, 0.5 and 0.1 from left to right) and Γ=8. Results with filled markers are the profiles of the average temperature in the layer thickness, whereas results with empty markers are the profiles at the surface of the layer.

Figure 6. Modelling of the radial temperature profile in the layer (averaged in z and φ) with the parameters T_p, r_p and s_p.

Based on the numerical results, combined with the global energy balance, the following correlation can be derived for the plateau temperature:

$$T_p = 1.2 Ra_\phi^{-1/5} \left(\Gamma(1 - R_f)\right)^{4/5} \quad (9)$$

It depends on the three governing parameters of the system. The dependence with the Rayleigh number and with the aspect ratio of the average temperature of the system (representative of the plateau temperature) is illustrated in Figure 7 for the different calculations performed for the case R_f=0.1. In [13], the scaling derived from the numerical results is theoretically explained with an analysis of the boundary layer along the cold wall. The dominant impact of the temperature difference between the bulk (representative of the plateau temperature) and the imposed T_0 temperature at the wall is demonstrated based on the consideration of the balance between buoyancy and viscosity in this layer.

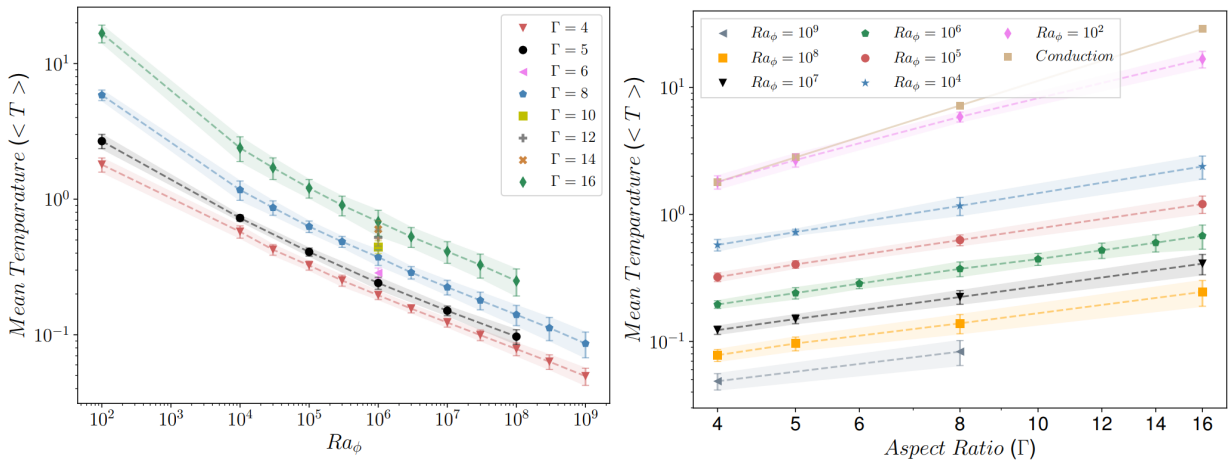

Figure 7. Log-log plot of the mean temperature evolution with Rayleigh number for different aspect ratios (left) and with the aspect ratio for different Rayleigh numbers (right). $R_f = 0.1$.

For the second part of the temperature profile, analysis of the results shows that the slope only depends on the Rayleigh number with the following correlation:

$$s_p = 4.37\, Ra_\phi^{-1/3} \tag{10}$$

This relation appears quite simple and seems to indicate that the linear increase of the temperature in this region is directly and only associated with the imposed heat flux at the bottom. Increasing Ra_ϕ reduces the relative temperature variation in the layer and reduces the slope of the radial temperature profile which indicates that the convection velocity increases. This was confirmed by the post-processing of the average radial velocity obtained in the simulations (cf. Figure 8): the radial velocity is uniform along the radius and does not depend on the aspect ratio nor on the heat flux ratio.

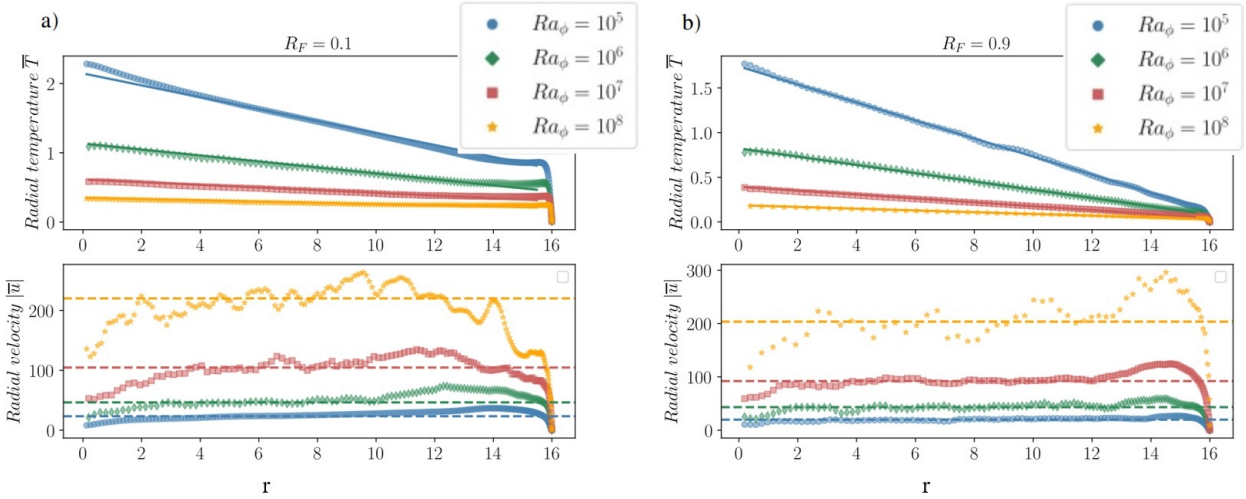

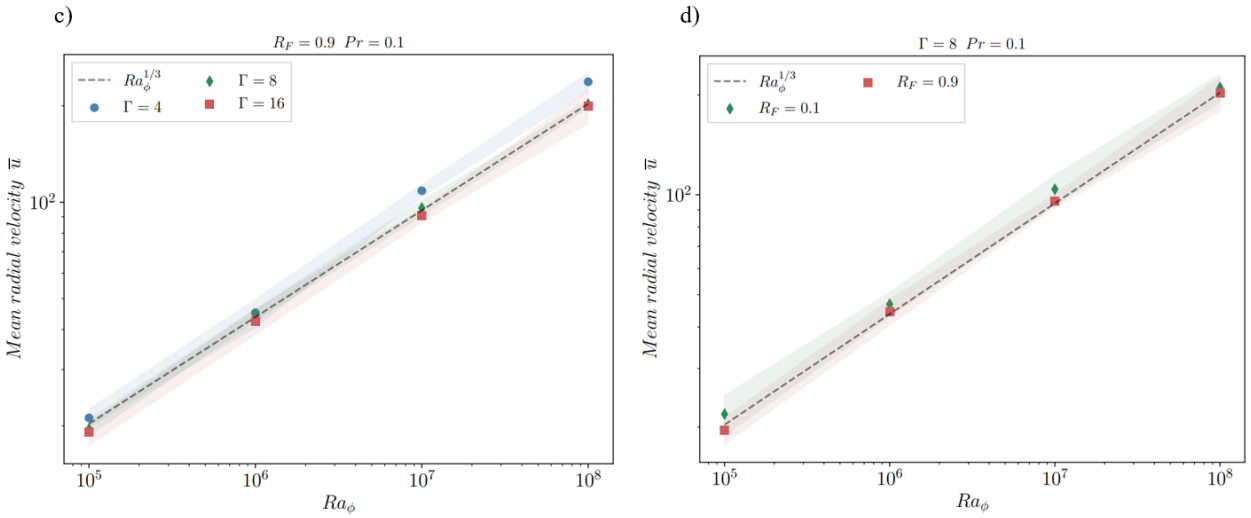

Figure 8. Scaling of the average radial velocity and link with the temperature slope in the central zone: a,b) Radial temperature and velocity profiles depending on the Rayleigh number for Γ=16 and a) $R_f = 0.1$ and b) $R_f = 0.9$; c,d) Scaling of the mean radial velocity with Rayleigh number c) at fixed R_f and d) at fixed Γ.

In Figure 9a), the length of the plateau zone in the radial temperature gradient near the lateral cooled wall is evaluated for a given aspect ratio and depending on the Rayleigh number and on the heat flux ratio. It is shown that, as observed in Figure 5, increasing the top heat flux leads to decrease this length. In Figure 9b), the influence of the aspect ratio is shown. Based on the simulations results the scaling law presented in equation (11) is derived.

$$\Gamma - r_p \;=\; \Gamma\left(1 - R_f\right)\left(0.03ln\left(Ra_\phi\right) - 0.31\right) + 0.365\Gamma^{0.432} \qquad (11)$$

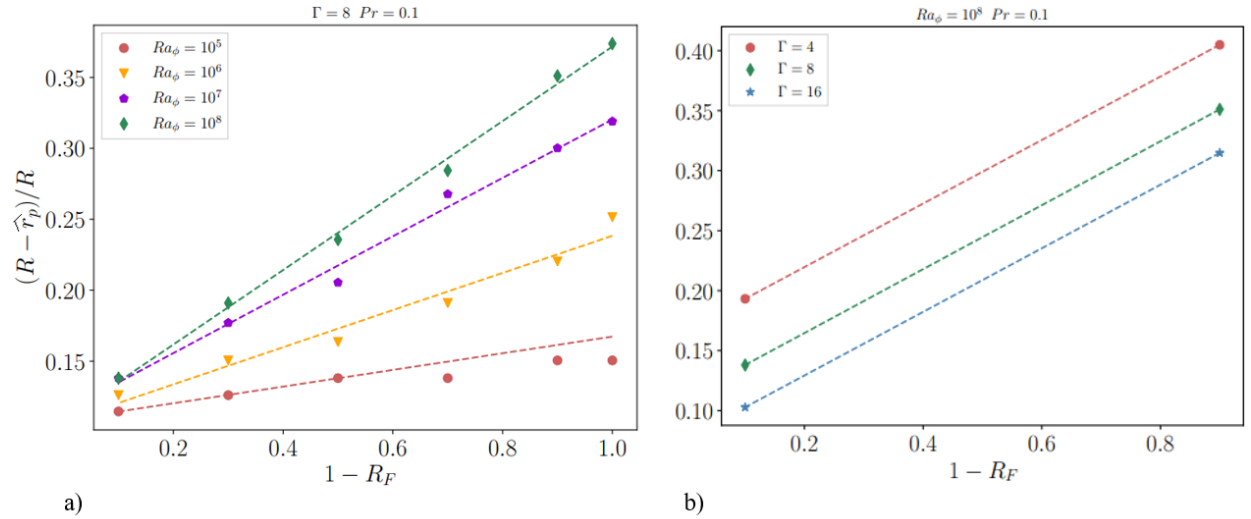

Figure 9. Length of the plateau zone in the radial temperature profile depending on the heat flux ratio and a) the Rayleigh number, b) the aspect ratio.

Based on this analysis, allowing to understand and evaluate the radial profile of the average temperature (averaged in z and φ) of the metal layer depending on its main characteristics (Γ, Ra_ϕ, R_F), it is proposed to derive a model for the radial profile of the temperature at the top surface $T_{up}(r)$ (averaged in φ at z=1). Since comparable profiles are obtained for the top surface temperature (cf. Figure 5 and Figure 10), the form of the correlations used for the analysis of the average temperature is kept, adapting only slightly the slope of the temperature profile and adapting the plateau value which may be higher or lower compared to the one of the average temperature depending on the heat flux ratio. Equation 11 for r_p parameter remains valid for the top surface temperature. The slope of the linear profile is derived from the simulations results, as well as the temperature plateau (i.e. the temperature when $r = r_p$). New correlations for the top surface temperature are given in equations (12) and (13).

$$s_p' = 5.59\ {Ra_\phi}^{-0.35} \tag{12}$$

$$T_p' = 1.1\left(1 - R_f\right){Ra_\phi}^{-0.2}\Gamma^{0.432} \tag{13}$$

Looking at the temperature profile in Figure 10, it is visible that the temperature plateau exists and plays a role only for cases with small heat flux ratio. Considering the plateau temperature when r>r_p for high heat flux ratios would lead to overestimate the surface temperature and consequently the top radiative heat transfer, which is not conservative regarding the lateral heat flux evaluation. This plateau can be introduced in the modelling for low heat flux ratio. However, evaluations have shown that its contribution remains limited compared to a linear decrease of the temperature (neglecting the plateau). Therefore, a radial linear profile for the top surface temperature using equation (14) is a reasonable and conservative approximation for all heat flux ratios.

$$T_{up}(r) = T_p{}' + s_p{}'.r_p.\left(1 - \frac{r}{r_p}\right) \tag{14}$$

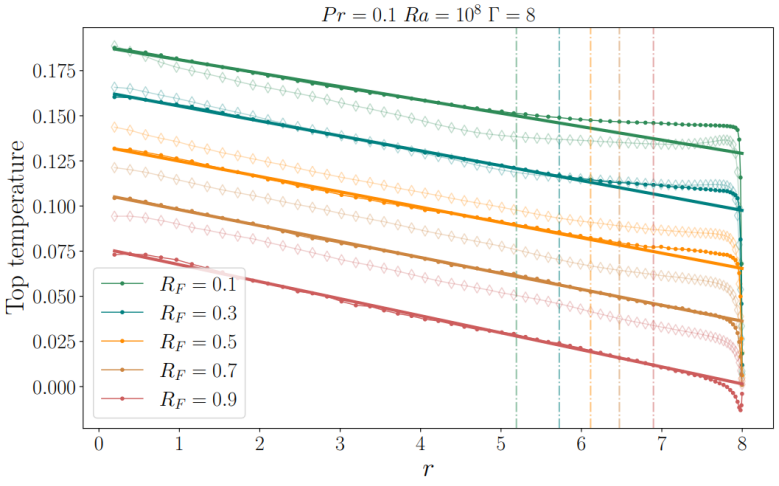

Figure 10. Radial temperature profile depending on the heat flux ratio, at the top of the layer (filled with colors) and average temperature in the layer thickness (only contours). Vertical lines indicate value of r_p for each R_F and continuous lines the slopes of the top surface temperature profiles.

4. A NEW HEAT TRANSFER MODEL FOR LUMPED-PARAMETER LOWER PLENUM CODES

Based on the understanding of the fluid behavior and on the scaling laws obtained for the temperature profile at the top of the metal layer from the DNS presented in the previous part (equations 11 to 14), a new model is proposed to simply estimate the power partitioning in the top metal layer in all possible configurations expected in the reactor case. Since in SA codes, the top radiative heat transfer is calculated based on the state of the surrounding structures, it is necessary to implement an iterative method to solve the problem. The algorithm presented in Figure 11 is proposed: Iterations are performed to converge on the value of the parameter R_f, defining an acceptance criterion ε. The radial temperature profile at the top surface of the system is calculated based on the knowledge of $\widehat{r_p}$, $\widehat{T_p'}$ and $\widehat{s_p'}$ considered here in their dimensional forms. This profile is then used to calculate the heat flux at the top of the layer.

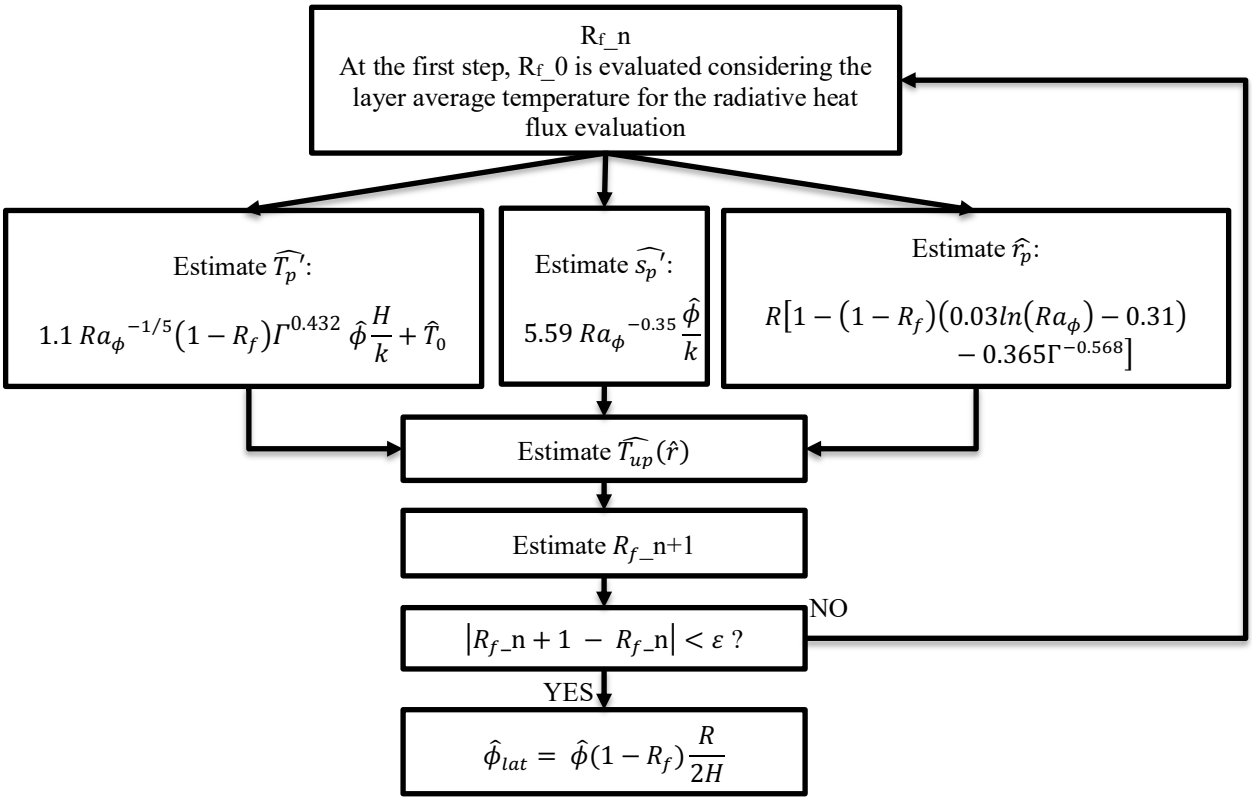

Figure 11. Algorithm for evaluation of heat transfer in top metal layer.

This new model is suitable for transient configurations when the top metal layer may become very thin or even disappear (due to stratification inversion) and better considers the impact of the top boundary condition on the fluid behavior thanks to the R_f parameter in the correlations. It should be noticed that when the layer height tends to 0, the plateau temperatures of both top and average temperature profiles tend to the boundary condition of $\hat{T}_0$, meaning that the lateral heat flux will also tend to 0. This behavior is obtained thanks to a lower exponent of H tending to 0 compared to R_f tending to 1, as shown in equations (15).

$$\begin{aligned}\widehat{T_p'}-\hat{T}_0 &\propto H^{-0.232}(1-R_f)\\ \widehat{T_p}-\hat{T}_0 &\propto H^{-3/5}(1-R_f)^{4/5}\end{aligned} \tag{15}$$

The limitation of 0D model [2] used up to now in SA code, associated to the lateral heat flux overestimation when the layer height decreases and identified with BALI-metal tests [6] is thus overcome thanks to this new modelling: for a thin metal layer, the temperature in the center of the layer increases at the same time as the one near the cold wall decreases. This behavior could not be captured using only one average temperature for the layer. It could be noted that another approach is proposed in MAAP code, to deal with this lateral heat flux reduction when the thickness decreases. It is based on a thermal eddy diffusivity model adapted to the metal layer configuration [14]. However, no results were presented to validate that approach.

In order to confirm the capacity of this simplified model to represent DNS results in terms of power partitioning in the metal layer, a given metal layer configuration was calculated with DNS and evaluated with the model considering the same simple top radiative boundary condition based on an average emissivity of 0.38 and a uniform environment temperature fixed at the melting temperature of steel $\hat{T}_0$. For this comparison, physical properties used are synthetized in Table II and a 2m radius vessel is considered. Please note that, in accordance with the methodology used in our study, the imposed bottom heat flux was chosen at a low value ($\hat{\phi} = 1kW/m^2$) compared to reactor case in order to limit the Rayleigh number for the DNS simulation. Since heat flux ratio is imposed in the DNS simulation, the radiative heat flux was calculated based on the real temperature profile calculated in the DNS simulation. As shown in Figure 12, a good agreement is obtained for both temperature profile at the top surface of the layer and radiative heat flux (underestimation of the time averaged value is equal to 1.5%).

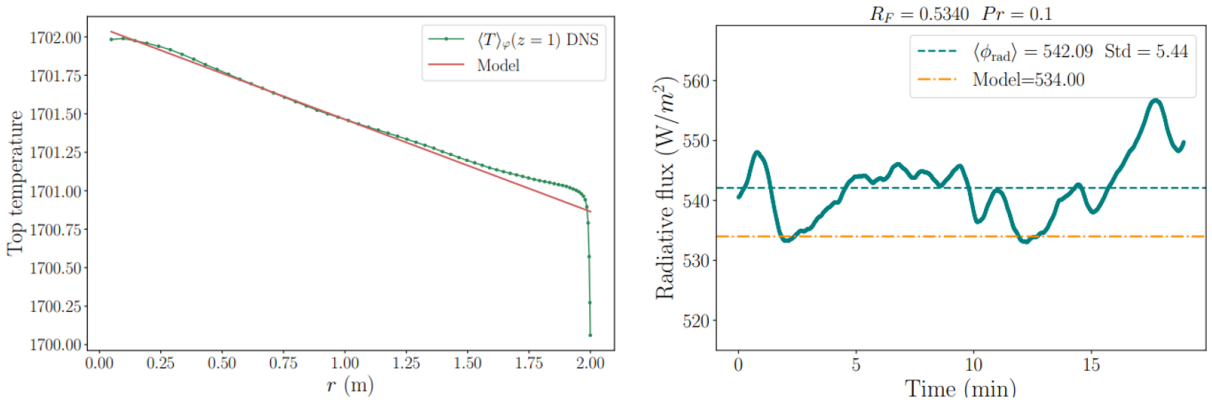

a) b)

Figure 12. Comparison between the model and the DNS simulation: radial temperature profile at the top of the layer in K (a) and radiative heat flux (b). Characteristics of the configuration: $\Gamma = 8$, $Ra_\phi = 4.22.10^7$, $Pr = 0.1$, $R_F = 0.534$, $\hat{\phi} = 1kW/m^2$,

Table II. Synthesis of physical properties of the metal layer used for dimensional evaluations.

Property	Value
Thermal conductivity	20 W/m/K
Heat capacity	450 J/K/kg
Dynamic viscosity	5.10^{-3} Pa.s
Density	7000 kg/m^3
Thermal expansion coefficient	10^{-4} K^{-1}
Melting temperature	1700 K

In Figure 13a), the results of the new model are compared with the ones of the original 0D model for different aspect ratios and considering the same simple top radiative boundary condition based on an average emissivity of 0.38 and a uniform environment temperature $\widehat{T_{inf}}$ fixed at the melting temperature of steel $\hat{T}_0$. The bottom heat flux is taken equal to 1MW/m² representative of the reactor case and physical properties of the metal are taken from Table II. For small aspect ratios, the overestimation of the lateral heat flux by the original 0D model is limited but it becomes visible for aspect ratio around 20, which corresponds to a metal layer of typically 10cm (the radius of the vessel being considered equal to 2m). However, when the radiative heat flux increases, the difference remains significant for larger metal layer, as illustrated in Figure 13b), where the impact of the possible presence of a thin layer of Zirconia at the surface which can enhance the emissivity up to 0.8 and of a lower environment temperature of 900K is estimated. It is shown that the evolution of the top boundary condition in the reactor case may have a significant impact on the risk of vessel failure in transient situation when the metal layer thickness is reduced. Indeed, not only the value of the maximum lateral heat flux is impacted but also the thickness below which the lateral heat flux decreases. It is particularly important for the integral codes, which predict the kinetics of increase of the top metal layer thickness, to capture well the transient increase of the maximum heat flux due to focusing effect and then decrease since the cumulated energy transferred to the vessel wall will have a direct impact on heating and progressive ablation.

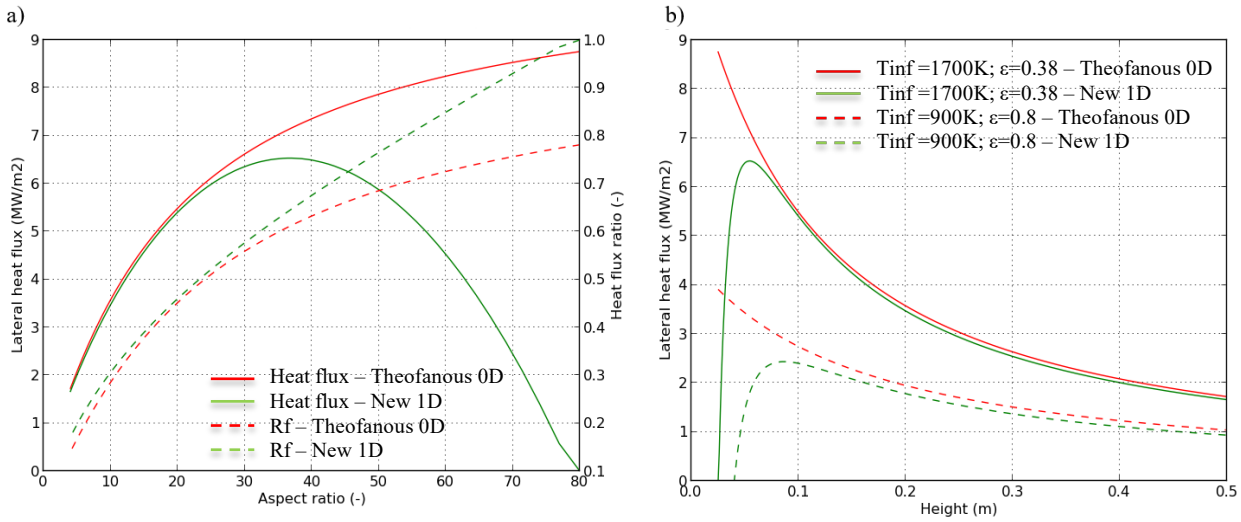

Figure 13. Comparison of the average lateral heat flux and heat flux ratio R_f evaluated with the new model and with the original 0D model from Theofanous [2] as a function of the aspect ratio (a) and impact of the radiative condition for various metal layer heights (b).

In Figure 14, the evolution of the average and maximum temperatures of the top surface of the layer depending on its thickness is presented. It is shown that for a thin metal layer, the consideration of the average temperature is not sufficient, since significantly higher temperature is expected in the center. This result shows that for thin layers (typically below 10cm) it may be necessary to consider in the evaluation the impact of other physical phenomena occurring in the hottest region, such as the melting of the oxide crust changing the assumption of uniform heat flux at the bottom or even the possible metal evaporation leading to speed up the metal layer disappearance.

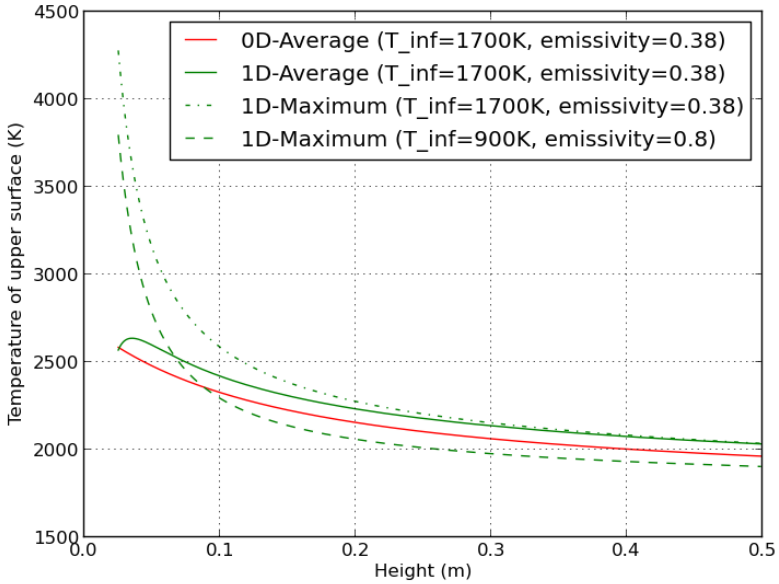

Figure 14. Average and maximum temperature depending on the layer height, effect of the model and of the radiative conditions.

5. CONCLUSIONS

DNS were performed for the 3D cylindrical metal layer, covering as much as possible the different layer characteristics expected in the reactor case, in terms of Rayleigh number, aspect ratio and top boundary condition. Those simulations were performed with the objective to better understand the fluid behavior and associated heat transfer in the layer for the different configurations. For that purpose, an assumption of uniform heat flux at the top boundary condition has been taken in order to decouple that condition from the temperature field, as a first step. The analysis revealed two zones in the layer: one on the cylinder edge influenced by the cooled lateral wall where the temperature averaged in axial and azimuthal directions is uniform, and the second one in the center where the temperature rises linearly due to the fluid horizontal motion and to the bottom imposed heat flux. The length of the lateral zone (cold side) and the temperature plateau near the cooled wall were identified as being influenced by the heat flux at the top of the layer. Based on the scaling laws derived from the numerical simulations, a 1D temperature profile along the layer radius has been proposed for the average temperature and for the one at the top surface, allowing an estimation of the radiative heat flux. An iterative method was used to solve the system (i.e., until reaching the consistency between flux-based correlations and temperature-based expressions of the heat fluxes) and is suitable for implementation in SA integral code. It was shown that this new model reproduces the results of DNS, with very limited conservatism regarding the lateral heat flux evaluation and can deal with transient evolution of the corium pool, without overestimation of the lateral heat flux when the layer thickness decreases. In addition, another advantage of this model lies in the evaluation of the 1D radial temperature profile, since heat flux lost by radiative heat transfer at the top of the layer plays a significant role on the heat flux partitioning in the layer, especially when the layer becomes thin. This opens the way towards a more precise evaluation with codes able to calculate the surrounding structures in the reactor and associated view factors with the top of the metallic pool. In particular, in the near future, this new model will be implemented in the SA integral code ASTEC [15] developed by IRSN in order to be coupled with the transient evolution of the metal layer height due to thermochemistry model and to the radiative model.
To further justify the applicability of this model to the reactor case, two complementary works are ongoing. The first one is a series of experimental tests in a dedicated device named FOCUS, allowing 3D representation of the cylindrical metal layer, using a simulant gas with representative Prandtl number. These

experimental results at higher Rayleigh numbers (up to 10^{10}) compared to DNS, will allow validating the extrapolation of the model done. The second one is the justification of the assumption of uniform heat flux considered at the top of the layer for the development of the model, especially for cases with high heat flux ratio. DNS simulations with top radiative boundary condition will be performed to quantify the impact on the fluid behavior.
The results given by the numerical simulations performed here are very rich and it is planned to use them furthermore to evaluate the lateral heat flux variations around its average value. In particular, the axial profile will be studied, as well as the azimuthal variation due to the break in the axisymmetry identified.

NOMENCLATURE

Dimensional variables
H Height of metal phase layer (m)
k Thermal conductivity (W/m/K)
R Radius of metal phase layer (m)
$\hat{P}$ Pressure of the fluid (Pa)
$\hat{T}$ Temperature of the fluid (K)
$\widehat{T_0}$ Imposed temperature of the lateral wall (K), taken at 1700K
$\widehat{T_{inf}}$ Uniform environment temperature above the metal layer (K)
$\hat{\boldsymbol{V}}$ Fluid velocity vector (m/s)
$\hat{u}$, $\hat{v}$ and $\hat{w}$ Fluid velocity in radial, azimuthal and axial directions (m/s)
β Thermal expansion coefficient (1/K)
κ Thermal diffusivity (m²/s)
ν Kinematic viscosity (m²/s)
ρ Density (kg/m^3)
$\hat{\phi}$ Heat flux imposed at the bottom of the metal layer (W/m²)

Non-dimensional variables
Pr Prandtl number
Ra_ϕ Rayleigh number based on imposed bottom heat flux ϕ
R_f Ratio between the heat flux at the top surface of the metal layer and the one imposed at the bottom surface
Γ Aspect ratio of the metal layer (ratio of radius to height)
P non-dimensional pressure of the fluid
T non-dimensional temperature of the fluid
$\boldsymbol{e_z}$ unit vector in axial direction

ACKNOWLEDGMENTS

Centre de Calcul Intensif d'Aix-Marseille is acknowledged for granting access to its high-performance computing resources. This work was granted access to the HPC resources of IDRIS under the allocations A0120407543 and A0140407543 made by GENCI. Commissariat à l'Énergie Atomique et aux Énergies Alternatives (CEA) and Électricité de France (EDF) are gratefully acknowledged for their financial support. This work was granted access to the Very Large Computing Center (TGCC) of the CEA under the allocation 32004148 made by IRSN to the Centre de Calcul Recherche et Technologie (CCRT).

REFERENCES

1. D. Tsurikov, "MASCA2 Project: Major Activities and Results", *Proc. of MASCA2 Seminar*, Cadarache (France), October 11-12, (2007).

2. T.G. Theofanous, C. Liu, S. Additon, S. Angelini, O. Kymaelaeinen, T. Salmassi, *In-vessel coolability and retention of a core melt*, Volume 1. Argonne National Lab (1996).
3. S. Globe, D. Dropkin, "Natural-convection heat transfer in liquids confined by two horizontal plates and heated from below", *J. Heat Transfer* **81**, pp. 24–28 (1959).
4. S.W. Churchill, H.H.S Chu, "Correlating equations for laminar and turbulent free convection from a vertical plate", *Int. J. Heat Mass Transf.* **18**, pp. 1323–1329 (1975).
5. C. Liu, T. G. Theofanous, *In-Vessel Coolability and Retention of a Core Melt*, Volume 1 appendix N, Argonne National Lab (1996).
6. J.M. Bonnet, J.M. Seiler, "Thermal hydraulic phenomena in corium pools: the BALI experiment" *Proc. Int. Conf. Nuclear Engineering* ICONE-7057, Tokyo, Japan (1999).
7. L. Carénini, F. Fichot, N. Bakouta, A. Filippov, R. Le Tellier, L. Viot, I. Melnikov, P. Pandazis, "Main outcomes from the IVR code benchmark performed in the European IVMR project", *Annual of Nuclear Energy*, **146** (2020).
8. L. Ma, J. Li, S. Ji, H. Chang, "Turbulent convection experiment at high Rayleigh number to support CAP1400 IVR strategy", *Nucl. Eng. Des.* **292**, pp. 69–75 (2015).
9. Z. Li, H. Chang, K. Han, F. Fang, L. Chen, "Experimental investigation on vertical heat transfer characteristics of light metallic layer with low aspect ratio", *Nucl. Eng. Des.* **377** (2021).
10. C. Le Guennic, E. Skrzypek, M. Skrzypek, B. Bigot, M. Peybernes, R. Le Tellier, "Synthesis of WP2.3 results on the metallic layer and new correlations", *Proc. of Int. Seminar "In-vessel retention: outcomes of IVMR project"*, Juan-les-Pins (France), January 21-22 (2020).
11. E. Skrzypek, M. Skrzypek, F. Fichot, "CFD study of heat transfer in a metal layer on top of the corium pool under severe accident conditions with prescribed top and bottom boundary conditions", *Proc. of the 19th Int. Topical Meeting on Nuclear Reactor Thermal Hydraulics (NURETH-19)*, Brussels (Belgium), March 6 - 11 (2022).
12. P. Fisher, J. Mullen, "Filter-based stabilization of spectral element methods" *Comptes Rendus de l'Académie des Sciences - Series I - Mathematics* **332** (3), pp. 265–270 (2001).
13. F. Rein, M. Le Bars, B. Favier, F. Fichot, L. Carénini, "Interaction between forced and natural convection in a thin cylindrical fluid layer at low Prandtl number" *Journal of Fluid Mechanics* **977**, A26, doi:10.1017/jfm.2023.922, (2023).
14. C. Y. Paik, S. J. Lee, J.H. Scobel, Q. Zhou, W. Luangdilok, R. W. Reeves, R. E. Henry, M. Plys, "In-vessel retention modeling capabilities in MAAP5" (NEA-CSNI-R--2012-2). *Nuclear Energy Agency of the OECD (NEA)*, July 2012.
15. P. Chatelard, N. Reinke, S. Arndt, S. Belon, L. Cantrel, L. Carénini, K. Chevalier-Jabet, F. Cousin, J. Eckel, F. Jacq, C. Marchetto, C. Mun, L. Piar, "ASTEC V2 severe accident integral code main features, current V2.0 modelling status, perspectives", *Nuclear Engineering and Design*, **272**, p.119-135 (2014).